Distribution Agreement

In presenting this thesis as a partial fulfillment of the requirements for a degree from Emory University, I hereby grant to Emory University and its agents the non-exclusive license to archive, make accessible, and display my thesis in whole or in part in all forms of media, now or hereafter now, including display on the World Wide Web. I understand that I may select some access restrictions as part of the online submission of this thesis. I retain all ownership rights to the copyright of the thesis. I also retain the right to use in future works (such as articles or books) all or part of this thesis.

Cristin Hendrickson April 10, 2018

Transcriptional Elongational Roadblocking by the Lambda Bacteriophage CI Protein

by

Cristin Hendrickson

Laura Finzi
Adviser

Department of Physics

Laura Finzi

Adviser

David Dunlap

Committee Member

Jed Brody

Committee Member

Jen Heemstra

Committee Member

2018

Transcriptional Elongational Roadblocking by the Lambda Bacteriophage CI Protein

By

Cristin Hendrickson

Laura Finzi

Adviser

An abstract of
a thesis submitted to the Faculty of Emory College of Arts and Sciences
of Emory University in partial fulfillment
of the requirements of the degree of
Bachelor of Sciences with Honors

Department of Physics

2018

Abstract

Transcriptional Elongation Roadblocking by the Lambda Bacteriophage CI Protein
By Cristin Hendrickson

Transcription is a crucial cellular process that must be regulated to ensure proper gene expression. To gain a more complete picture of the control mechanisms, this experiment studies the effect of the lambda bacteriophage CI protein as a roadblock to transcriptional elongation. Using Atomic Force Microscopy, images were taken of DNA, RNAP and the lambda repressor with nanometer resolution. Based on the location of the RNAP and the roadblocks, the effect of CI on transcriptional elongation was then determined. An initial distribution of these positions showed that CI oligomers on unlooped molecules are not effective roadblocks for RNAP while CI oligomers that mediated loops block elongation. Specifically for CI, binding at the near operator, with respect to the promoter, occurred on average 389 bp away from the start of the DNA with a standard deviation of 22 and binding at the far operator occurred on average 879 bp away from the start of the DNA with a standard deviation of 32. Statistically, on unlooped molecules RNAP was found an average of 390 bp away from the start of the DNA with a standard deviation of 246. On looped molecules, RNAP was found an average of only 214 bp away from the start of the DNA with a standard deviation of 118. This difference initially suggested the topology of the DNA-protein complex determined to what extent a CI in the path of an elongating RNA polymerase interfered with transcriptional elongation. However, only 23 looped molecules were analyzed in contrast to the 46 unlooped molecules that were used. The categorization data for CI binding and topology then showed that transcription interferes with looping by reducing the percentage of looped molecules from 55 percent in the control to 6 percent in the samples with regulated transcription. Additionally, transcription increased the percentage of molecules without any bound CI oligomers from 15 percent in the control to 64 percent in samples with regulated transcription. This additional analysis then suggests that lambda oligomers are not significant obstacles for transcription which in fact disrupts them. In that case, for the lambda repressor to maintain control of the lytic/lysogenic switch, genes nearby might be organized to diverge, so that elongating polymerase do not disturb lambda repressor oligomers holding the switch.

Transcriptional Elongation Roadblocking by the Lambda Bacteriophage CI Protein

By

Cristin Hendrickson

Laura Finzi

Adviser

A thesis submitted to the Faculty of Emory College of Arts and Sciences
of Emory University in partial fulfillment
of the requirements of the degree of
Bachelor of Sciences with Honors

Department of Physics

2018

Acknowledgements

Many thanks to Zsuzsanna Voros, Dr. Finzi and Dr. Dunlap for their guidance and expertise.

Funding was generously provided from NIH GM084070 to L.F. and D.D.

Table of Contents

Table of Figures

I. Introduction

A. Transcription as a Key to Life

Transcription is an important cellular process and essential to life itself. It is the first step in gene expression and leads to the production of proteins. During transcription, RNA polymerase (RNAP) (Fig. 1) uses one strand of double-stranded deoxy-ribonucleic acid (DNA) to create a ribonucleic acid (RNA) molecule which is then modified to move outside the nucleus to serve as the code for the ribosome to synthesize proteins.

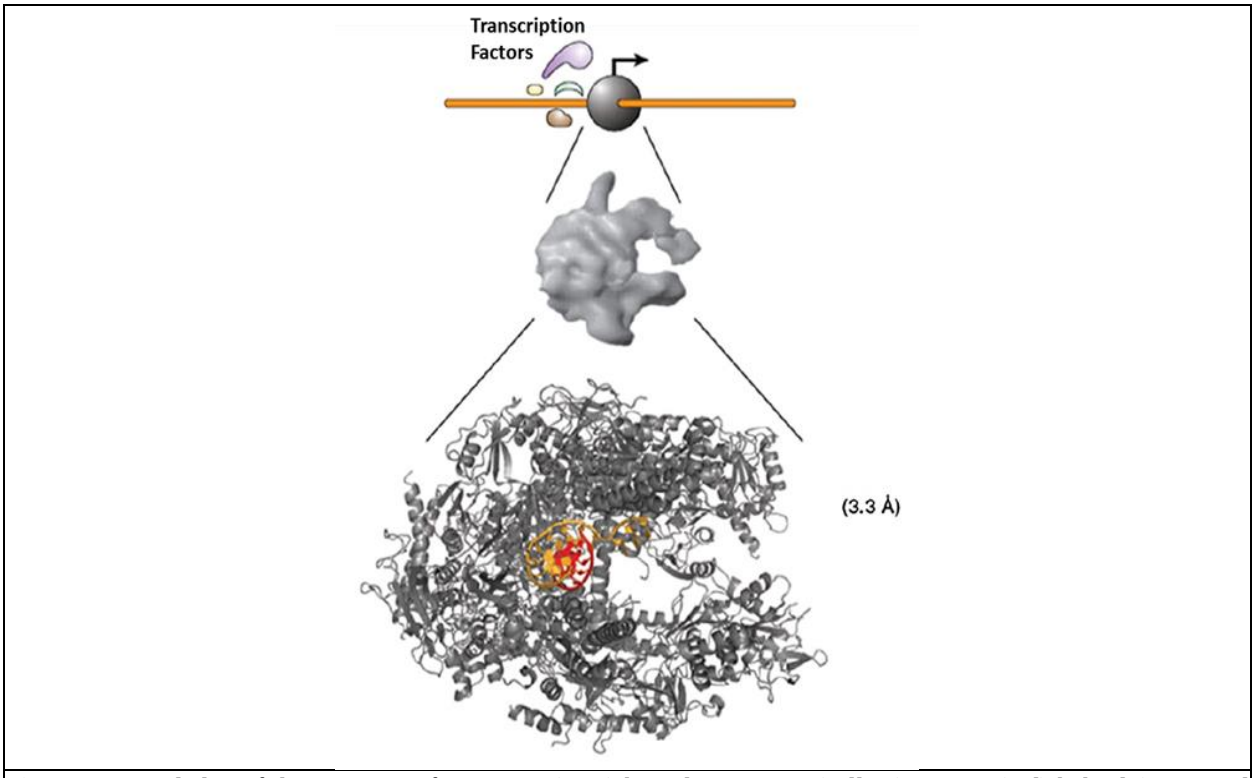

Figure 1 Knowledge of the structure of RNAP II (gray) bound to a DNA (yellow) - RNA (red) hybrid (Reprinted with permission from Ansari Copyright 2007 Nature Chemical Biology).

Transcription can be divided into three main steps: initiation, elongation, and termination (Fig. 2). In initiation, RNAP recognizes a promoter sequence along dsDNA and separates the two strands from each other, so that RNAP can bind to the template strand. Elongation is the process by which

RNAP travels along the DNA strand and matches each of its deoxy-ribonucleotide with a ribonucleotide produce a chain of RNA. Finally, termination occurs when the RNAP encounters a terminator sequence of DNA. Transcription then stops, and the RNAP dissociates from DNA.

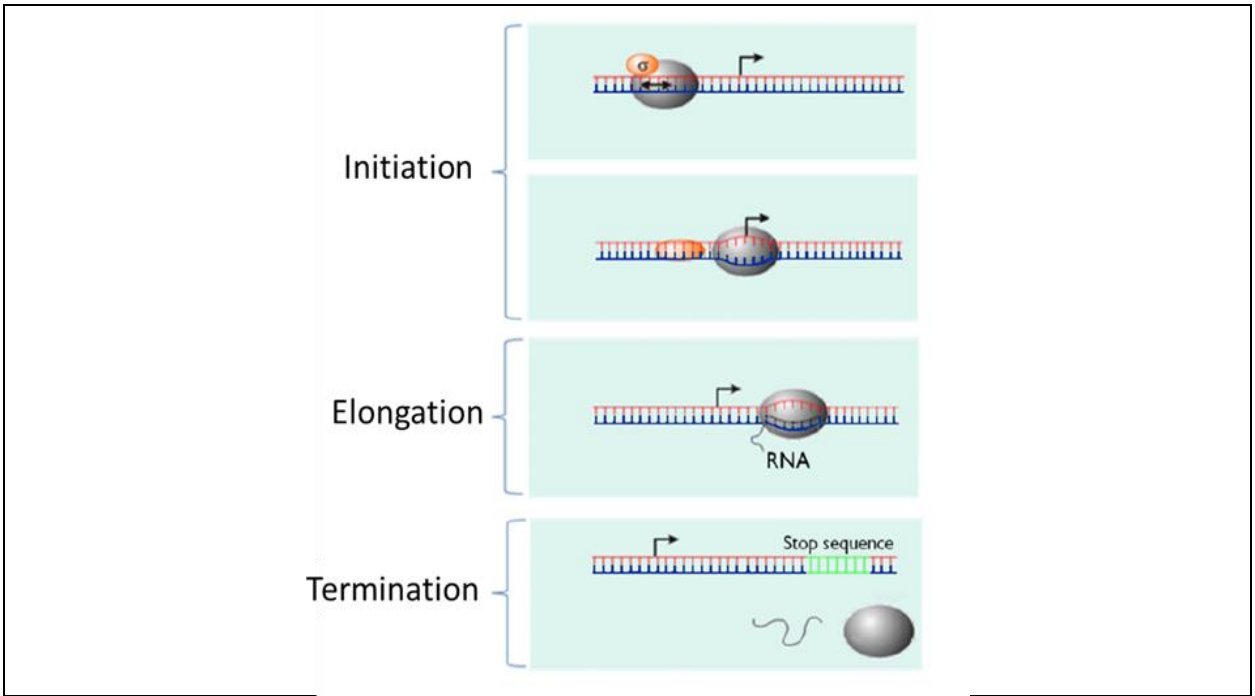

Figure 2 Transcription cycle of RNAP in the *E. coli* bacterium. RNAP is the gray sphere and the two DNA strands are the red and blue lines (Reprinted with permission from Billingsley Copyright 2007 Physical Biology).

Meanwhile, the RNA chain undergoes post-transcriptional modification to prepare it for use as a coding sequence for a protein (Billingsley 2012).

B. Lambda Bacteriophage as a Model for Transcription Regulation

Since transcription is ubiquitous in biological kingdoms, what can be learned about it in a simple model system like the lambda bacteriophage is relevant to more complex life forms. When the lambda bacteriophage infects a host bacterium, it exhibits two different modes of propagation. In the lytic state, the phage hijacks the cell's transcriptional process to produce more bacteriophages and then releases them via lysis into the extracellular environment to infect more cells. Alternatively, in the lysogenic state the phage is assimilated into the host DNA and is propagated to daughter cells during mitosis. This state is maintained by the activation of transcription at the PRM promoter and by the repression of the lytic genes controlled by the PR

promoter. In particular, transcription at PRM produces a CI protein, the dimeric form of which is called the lambda repressor and is responsible for suppressing the lytic genes. When the DNA is damaged, the protein RecA is activated to cleave the lambda repressor, so the transcription rate for CI drops and the lytic genes are no longer repressed (Ptashne 2004). More specifically, CI cleavage separates the N terminal domain from the C terminal domain and creates monomers which no longer have the affinity needed to bind to the operators that are responsible for repressing lysis (Ptashne 2004 and 2008). After CI cleavage, transcription at PR may proceed and the protein Cro is produced which blocks the PRM promoter. Cro is continually produced until it reaches a concentration at which it becomes so saturated that its binding prevents RNAP from accessing PR. At that point, transcription begins at PRM and the lysogenic state takes over (Ptashne 2004). Therefore, the state of the lambda phage is a direct result of the activation and repression of genes by the proteins CI and Cro.

Looking more closely at the lambda repressor, its structure is directly responsible for the repression of the lytic genes. Conceptually, CI is dumbbell shaped with two distinct domains that are connected via a protease sensitive connector (Fig. 3). However, there is no axis of symmetry as the NTD and CTD are almost orthogonal (Stayrook 2008).

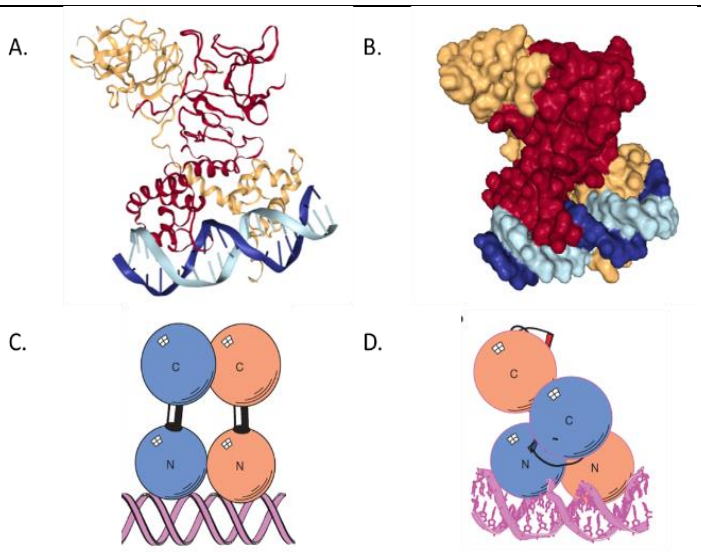

Figure 3 A & B Two different representations of the crystal structure of the lambda repressor (Rose 2015) **C & D** A representation of the lambda repressor bound at an operator. One subunit is colored salmon with a red cleavage site region while the other subunit is colored blue with a dark blue cleave sight region. N and C stand for the NTD and CTD respectively. C is a cartoon representation while D shows the relative positions of the NTDs and CTDs based on the crystal structure (Adapted with permission from Stayrook Copyright 2008 Nature).

Dimers are formed from the weak self-association of the NTDs which are also responsible for binding to the operator sites while the CTD underlies cooperatively (Ptashne 2004). More specifically, the structure of the dimer allows it to adopt a conformation which leads to pairs of dimer cooperatively binding at adjacent operator sites. For example, there are interactions between the cleavage site region (CSR) and the NTD of the dimer related subunit which leads to asymmetric dimer assembly. As shown in Fig. 4 the NTD of the orange dimer is further apart than the NTD of the blue dimer which allows cooperative binding to occur between the CTDs since it positions them in a manner where they can bind.This asymmetric dimer assembly then leads to the corporative ‘alternative pairwise’ binding that occurs at adjacent operator sites since it positions the CTD in the middle so it can connect with another dimer.

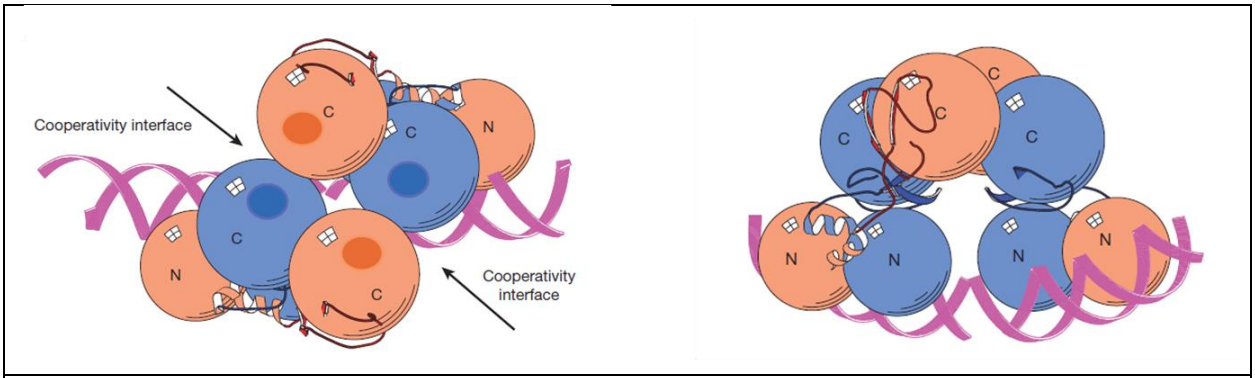

Figure 4 Two different views of the cooperativity complex of the lambda repressor. The right image is a 90 degree rotation about the horizontal axis of the left image (Adapted with permission from Stayrook Copyright 2008 Nature).

Similarly, octamers and loops are formed as a result of the CTD positioning of the tetramers (Stayrook 2008). Thus, the structure of CI is responsible for cooperativity and repression of the lytic state.

The previously mentioned lytic repression comes as a direct consequence of CI binding to different recognition sequences, operators. In the lambda bacteriophage, there are two operator regions (Fig. 5). The OR region has OR1, OR2, and OR3 and is bordered by PR on one side and PRM on the other. The OL region has OL1, OL2, and OL3 and PL which acts similar to PR and controls transcription of the lytic gene (Ptashne 2004).

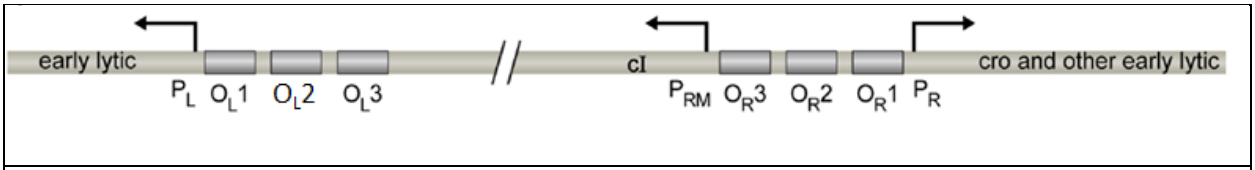

Figure 5 Layout of the lambda bacteriophage DNA (Adapted with permission from Hochschild Copyright 2009 Curr Opin Struct Biol).

CI binds cooperatively to the operator sites with the following order of affinity: OR1=OR2=OL1=OL2>OL3>OR3 (Meyer II 1980). The way the proteins are bound to these operator sites then directly affects gene expression and the lytic/lysogenic state of the phage. More specifically, binding at OR1 or OR2 or both represses PR and the lytic state while binding at OR1 and OR2 fully stimulates PRM and the lysogenic state (Fig. 6) (Meyer II 1980). This stimulation is promoted by binding at OR1 which cooperatively stabilizes binding at OR2 to establish contact with polymerase at PRM that activates transcription (Meyer III 1980).

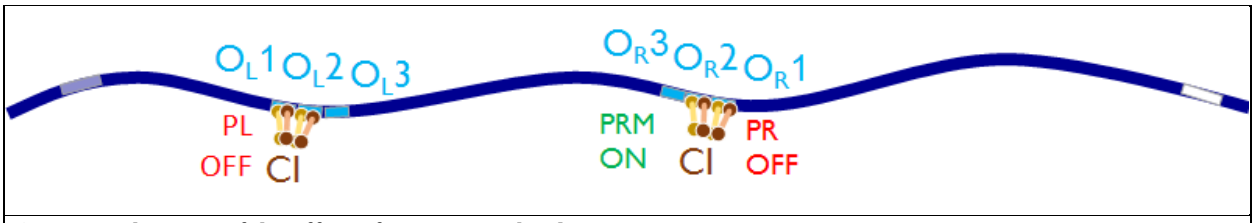

Figure 6 Schematic of the effect of CI operator binding on transcription.

If CI levels rise and binding occurs at OR3, PRM is then repressed (Meyer II 1980). However, once CI levels drop, PRM can again be activated and enhanced by cooperative binding at OR2. Interestingly, cooperativity occurs in *cis* between OR1 & OR2 but in *trans* between OR1& OR2 and OL1 & OL2 which allows individual sites to be occupied at lower CI concentrations (Lewis 2011). Consequently, the cell can maintain a stable lysogenic state even under various environmental conditions because of its activation and repression of the lysogenic genes.

Additionally, CI binding at operators can change the shape of the DNA and have a direct impact on the phage. For instance, two DNA sites in a relaxed unlooped state can move relative to each other and potentially form loops at rates of 0.5-2 s-1. These loops form approximately 72% of the time for wild type (OR & OL containing) DNA with a change in free energy for tetramers of -3.0 kcal/mol and a change in free energy for octamers of -0.5 kcal/mol (Hensel 2013). In order to form these long-distance, DNA loops, four dimers can bind to form an octamer (Fig. 7) that increases the stability of the CI protein on the operators (Revet 1999).

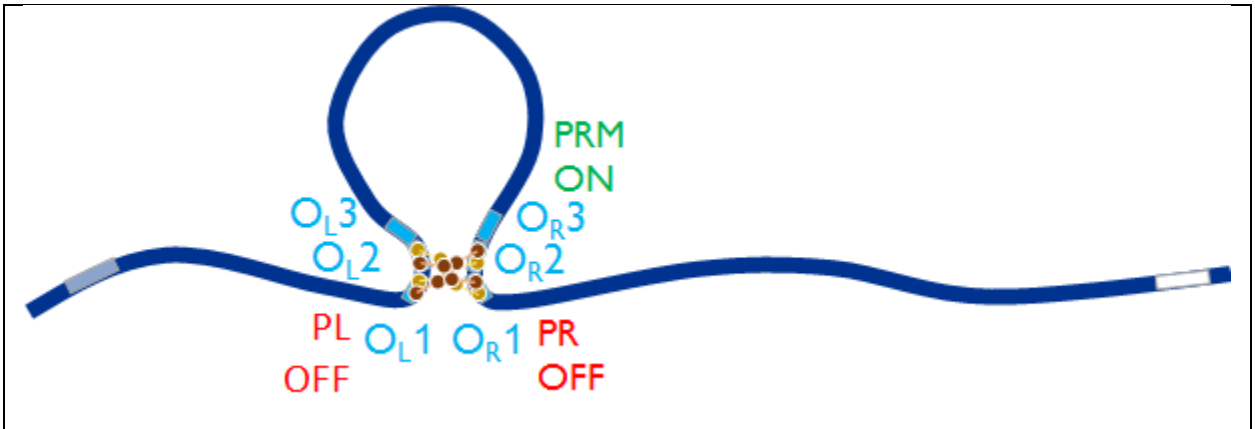

Figure 7 An octamer DNA loop formed by CI binding to OR12 and OL12.

As a result, looping activates PRM 2.4-fold with respect to the unlooped level (Hensel 2013). It is thought that this is a result of an interaction between α-CTD of RNAP at PRM and an UP element

located just to the right of OL3 which are brought into contact through antiparallel loop configuration. But it could also be that loops more tightly bind CI to OR2 (Lewis 2011). Therefore, octamer-stabilized looping functions to both enhance the lysogenic state and fortify repression of the lytic state.

However, the type and function of the loop can change depending on the CI levels. Under normal lysogenic concentrations of CI, a dimer does not have a high enough affinity to interact with the first and second operator sites (Zurla 2009). Loops only form when monomer CI levels increase to a physiological concentration of 200 nM in a lysogenic cell, which as previously mentioned enhances PRM and represses PR (Lewis 2011). However, excessively high CI levels can have a harmful effect on the cell by preventing it from effectively switching to the lytic state (Dodd 2001, 2004). Interestingly, at high CI concentrations, PRM is repressed as a result of OR3 filling in (Fig. 8). Although linkages between the corresponding O1 and O2 operators at OL and OR is sufficient to form a loop, a third linkage between dimers bound to O3 operators at OL and OR stabilizes the loop through head to head interactions of an additional tetramer (Zurla 2009). This is a natural consequence of the octamer-stabilized loop at OL12 and OR12 that brings OL3 and OR3 into close proximity and increases the probability that CI will bind at OL3 and form a link to OR3 (Dodd 2001).

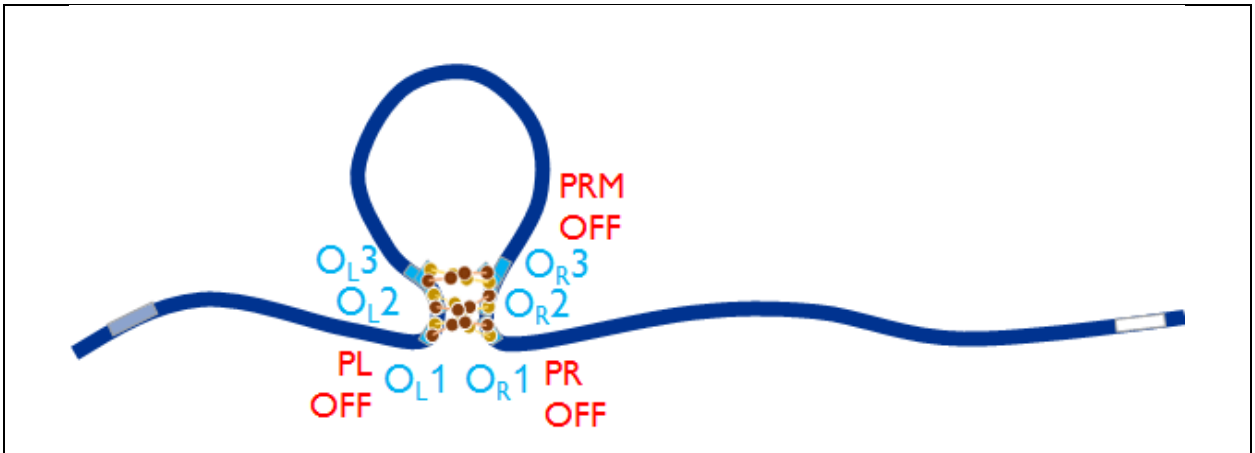

Figure 8 An octamer + tetramer DNA loop formed by CI binding to OR123 and OL123.

Since OR3 has poor intrinsic affinity, cooperativity with OL3 is necessary for CI to bind to it at normal concentrations (Lewis 2011). Without the formation of a tetramer at OL3 and OR3, PRM would likely not become repressed and CI levels might reach excessive levels (Dodd 2001, 2004). Consequently, looping helps the lysogenic state remain stable by repressing PRM when CI gets too high and enhancing it at lower CI levels.

C. Motivation for the Study of the Looping of Lambda Bacteriophage

As mentioned in the previous two sections, transcription is a key component of life that must be regulated to maintain homeostasis. To learn about more complex forms of life, it is expedient to study transcriptional regulation in simpler, model systems. The lambda bacteriophage is one such model system that has been used to understand genetic switches that are governed by loops, as the underlying mechanics of CI protein binding and loop formation of the lambda phage are well understood. However, for a more complete picture we seek to understand specifically how the CI roadblock affects transcriptional elongation. By studying this question we will gain more insight into the details of how genetic switches have evolved to employ loops in controlling genes.

II. Atomic Force Microscopy

A. Background

Scanning tunneling microscopy is a technique developed in 1983 that provides the topographies of surfaces in real space on an atomic scale. It consists of a tip, which is fixed to a piezodrive, scanned over a surface (Fig. 9). The piezo regulates the separation between the probe and the surface but requires a surface with excellent vibrational damping to maintain separations of several angstroms.

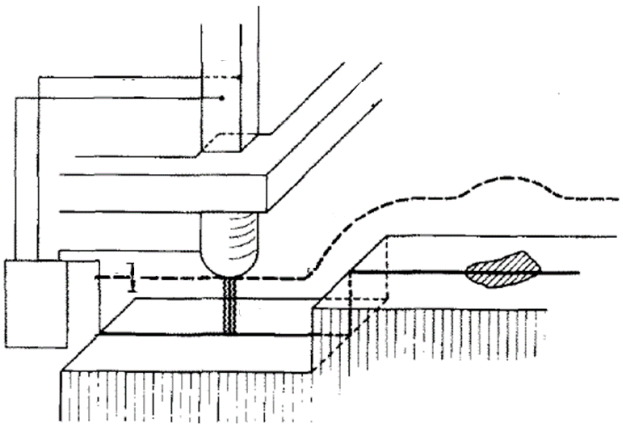

Figure 9 Early schematic of the scanning tunneling microscope (Adapted with permission from Binning Copyright 1983 Surface Science).

Lateral resolution of the image is determined by the radius of curvature of the tip. When the scanning tunneling microscope was developed, tips with a visible radius of curvature less than 1 μm were used. However, the edges were not straight which lead to several minitips on the tip itself. These minitips in turn improved the lateral resolution to 10 - 20 A. Meanwhile, depth resolution at the time of development was in the sub-A range (Binning 1983).

The atomic force microscope (Fig. 10) later came into being as an amalgam of the scanning tunneling microscope and the stylus profilometer. Like the scanning tunneling microscope (STM), the stylus profilometer is able to generate a 3D image based on the topography of the sample. However, it uses a cantilever to move a stylus over a surface to create an image. Early atomic force microscopy (AFM) combined these two imaging techniques by using the scanning tunneling microscope to determine the vertical displacement of the cantilever.

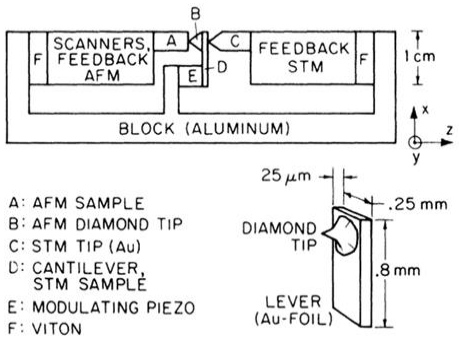

Figure 10 Early experimental setup of the atomic force microscope (Adapted with permission from Binning Copyright 1986 Physical Review Letters).

In contrast to its predecessor, its probe does not require a current through the surface. The spring

employed must be soft to deflect without exerting damaging force, but at the same time should be stiff to minimize the noise due to vibrations. To overcome this apparent contradiction, the spring constant and the mass of the spring are kept low. At the time of development, spring mass was 10-10 kg while the resonant frequency was greater than 2 kHz. Four different imaging modes based on two different feedback circuits could also be achieved. These factors led to a lateral resolution of 30 A and a vertical resolution of less than one A. Furthermore, it led to the ability to measure displacements of 10-4 A with forces of 2x10-16 N (Binning 1986).

B. Mechanics

Today, the atomic force microscope is one type of scanning probe microscope which measures interactions in the x-y plane and deflections up to 10 μm in the z direction. These electrostatic and Van Der Waals interactions occur between a microfabricated stylus at the end of a cantilever and a sample and are subsequently used to map a 3D image of the surface. The main components are a scanner, a sample holder, a stylus attached to a cantilever, and a deflection detecting system (Braga 2011). The cantilever is driven by a piezoelectric element at a particular frequency while the sample itself is positioned under the tip (Binning 1986). Additionally, the scanner is responsible for moving the tip and sample relative to each other via a digital control system. If the tip is moved it is classified as a scanning probe microscope but if the sample is moved it is classified as a scanning sample microscope. Nanometric positioning is achieved using piezoelectric ceramic materials which move in response to an applied voltage (Braga 2011).

When the tip and the sample are brought into close proximity, electrostatic and van der Waals forces cause the cantilever to bend. As the tip moves laterally over the sample, an image is created based on the deflections of the cantilever (Binning 1986 and Braga 2011). More specifically, a laser reflected off the cantilever to the center of a quadrant photodiode reveals the deflection of the tip as excursions of the laser spot across the photodiode (Fig. 11). The force

between the sample and the tip can be determined based on the cantilever deflection.

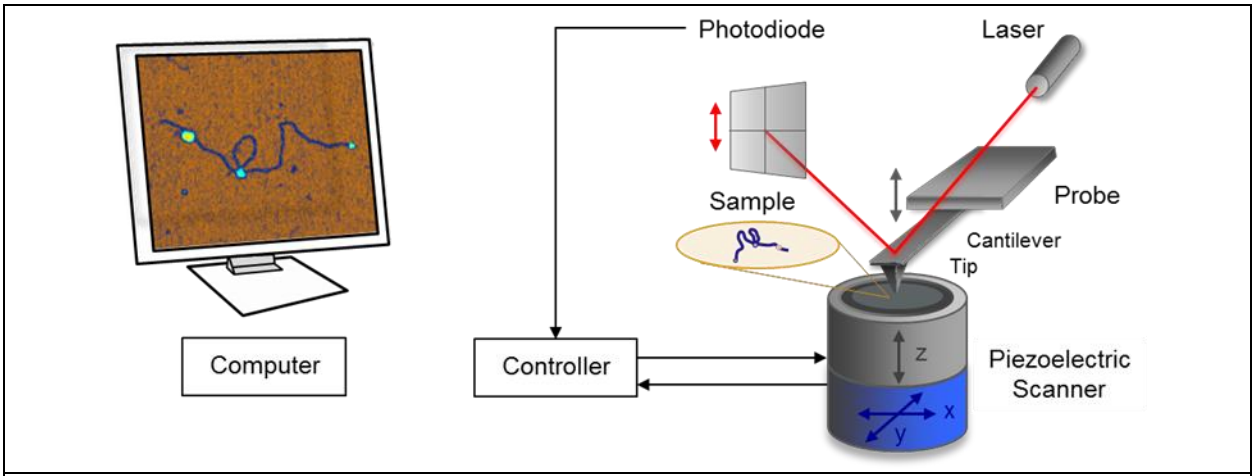

Figure 11 Schematic of a modern atomic force microscope (Courtesy of Z. Voros).

Interestingly, it is this optical lever method which allows picometer resolution in the z direction since it magnifies motions of the tip. In particular, a high amount of sensitivity to tip motion exists because the distance between the cantilever and photodiode is three times bigger than the length of the cantilever (Braga 2011). However, for the entire setup to work, the cantilever must be very close to the sample surface since the intermolecular forces that cause the deflections are very short ranged (Billingsley 2012).

The cantilever and tip are commercially available and can be purchased with the desired radius of curvature, aspect ratio, conductivity, magnetism and reactivity (Braga 2011). Tips can also be modified by chemical or adsorptive functionalization to measure properties such as binding or rupturing forces (Kreplak 2016). Relatively easy control and position of the cantilever is achieved through the chip that houses it. Typically, there are two major types of cantilever, the "V" shaped and the rectangular variety, each of which have different torsional properties (Fig. 12).

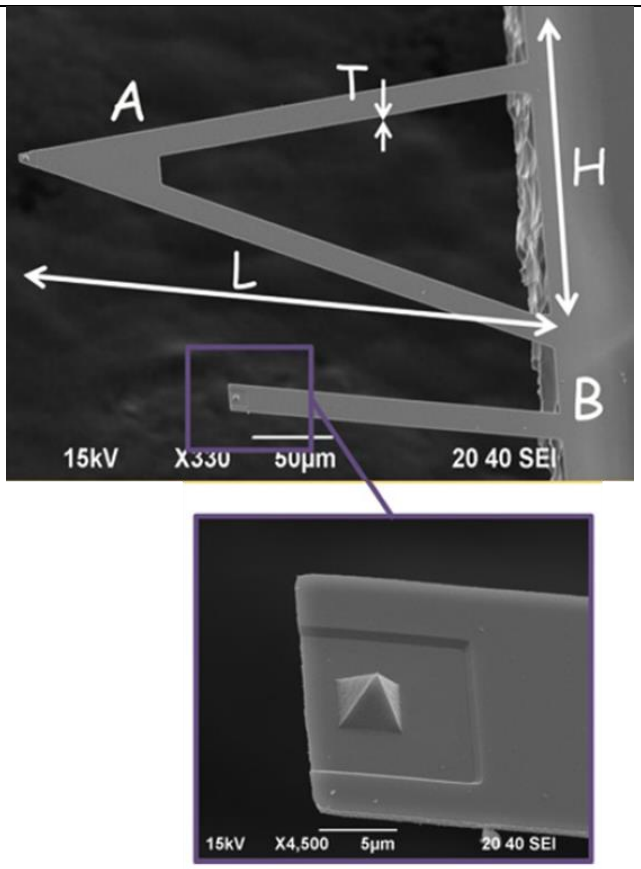

Figure 12 A Image of a "V" shaped cantilever. L is length, H is height, and T is thickness. **B** Image of a rectangular cantilever (Reprinted from Braga Copyright 2011 Humana Press).

Depending on the operating mode and experiment, cantilevers of different size are preferred. For samples using contact or resonance mode in liquid, soft, low-resonance ones are better. For imaging in air, stiff and high-resonance frequency cantilevers are better (Braga 2011). Commercially, cantilevers are made from silicon nitride and for biological application are 100-200 um in length with a spring constant of 0.01 - 0.05 N/m. In intermittent contact modes in which the cantilever oscillates as it moves over the sample, they usually operate close to their resonance peak (Kreplak 2016).

When AFM was first developed, tips were made from diamonds and glued on. Now however, tips are made from silicon or silicon nitride and can be microfabricated on the cantilever. Besides selecting the material, it is also important to consider the radius of curvature and aspect ratio of the tip (Fig. 13). It should be noted that sharper tips do not always obtain the best images as penetration of soft samples can occur and with smaller the apex radii, the tips will be more

fragile and may erode (Braga 2011). Standard tips have a radius of curvature of approximately 20 nm (Kreplak 2016).

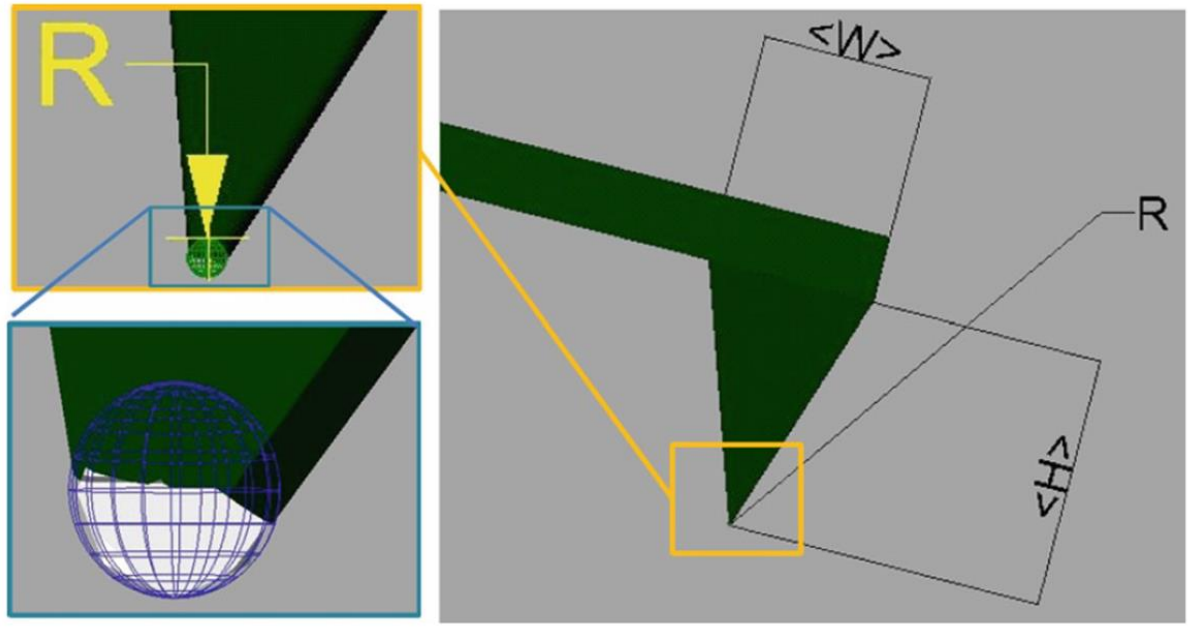

Figure 13 Schematic of a tip with radius of curvature R and aspect ratio H/W (Reprinted from Braga Copyright 2011 Humana Press).

Moving on to the mechanics, in the scanning sample atomic force microscope, the sample is attached to the scanner so there is easy access to the tip and scanner as a result of the afforded independence between the scanner and lever. However, the sample cannot be too large or heavy since the sample and scanner are connected (Braga 2011). Features of the sample can appear broader or shallower than they actually are, because the cantilever registers deflections that result from the convolution of the shape of the stylus with the topography of the sample. This is particularly evident when a stylus has multiple apexes and can contact the sample in more than one point at a time. Such a probe produces an image with duplicate features along the axis of the apexes. In addition, the tip shape may change if molecules become adsorbed and loosely adsorbed molecules may cause smearing. In such cases, one can try to clean the tip by scanning an open area with a large force or can just replace the tip (Kreplak 2016).

During imaging, a feedback loop is responsible for keeping the force of interaction between the stylus and the surface small and constant (Binning 1986). This system is composed of the

scanner, an electronic feedback circuit, the sample, the cantilever and optical lever (Fig. 14). Together these parts allow the atomic force microscope to measure and control the force on the sample so that low forces can be used to produce topographic images with minimal damage to the sample as the piezoelectric scanner moves the sample in a raster pattern. Throughout the scan, the feedback circuit modulates the voltage of the vertical drive of the scanner to move the sample up and down to allow the stylus follow the topography of the surface while keeping the interaction force (cantilever deflection) constant. The topographic image that results is is actually a record of the drive voltage sent by the feedback circuit to the vertical axis of the scanner. As a check, the images obtained from the trace and retrace of one line should be nearly identical, and if not, it might be due to a problem such as tip contamination or sample modification.

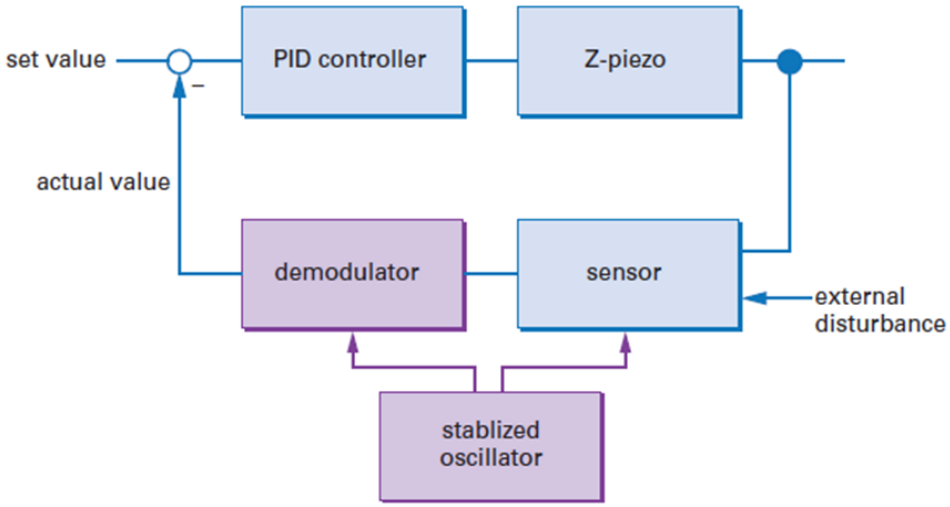

Figure 14 Diagram of the feedback loop. The set value is the imaging force the user chooses to operate the atomic force microscope at while the Proportional Integral-Differential (PID) feedback controller drives the Z-piezo to get the actual value as close to the desired set value as possible (Reprinted from Bruker Copyright 2011 Bruker Corporation).

Data obtained from the process is usually encoded on a color scale for visualization of the information obtained (Braga 2011).

C. Imaging

Originally, all atomic force microscopes were similar and built to measure flat, dry samples. Now however, the machines can be modified to make a variety of specialized

measurements such as imaging in liquid, unfolding and bonding interactions, and stretching of DNA and protein filaments (Braga 2011 and Kreplak 2016). Additionally, a wide range of samples can be studied with it, including but not limited to proteins, nucleic acid molecules, membranes and live cells (Kreplak 2016). Therefore, it is important to have a clear goal in mind when using AFM so the appropriate settings and features can be utilized to produce the best image (Braga 2011).

When imaging biological samples, the forces between the tip and sample should be at a minimum, since these samples are often soft and fragile. Additionally, the pH and ionic strength of the buffer solution can interfere with the interacting forces between the tip and the sample, so buffer conditions with a pH near 7.3 and an ionic strength around 100 mM often work best. Choosing buffers with low ionic strength can also minimize hydrophobic and hydrophilic interactions. Similarly, when imaging proteins weakly adsorbed to a surface, forces exerted on the sample should be minimized and optimal buffer conditions should be selected (Kreplak 2016). It is important that the sample be securely attached to the scanner during imaging, so there is no blurring. Samples imaged in air are attached to a sample support such as a mica glued to a ferrous metal disk that can be held in place magnetically on the piezoelectric scanner.

Sample preparation is simple and straightforward, but care should be taken to avoid fingerprints, dust, scratches, etc., so that a clear image can be obtained. Often it helps to wear gloves, handle the sample with tweezers, and clean the surface with dry gas (Braga 2011). If they aren't prepared well, samples can cause vibrational oscillations that degrade the image quality (Kreplak 2016). Additionally, artifacts either from the tip, the scanner, the environment, the control system, or the imaging processing software can affect the image (Braga 2011). As a result, mica is often used since it produces few image artifacts on account of being atomically flat. It can also be cleaved with tape before each image is taken so there is a clean, smooth surface for each sample

examined (Kreplak 2016). During imaging, there is minimal sample damage which allows resolution between sub nanometer to 100 μm in a variety of different environments such as air, liquid, or vacuum.

Although it is beyond the scope of this thesis, it should be noted that an AFM can be used for more than just imaging including but not limited to pushing, pulling or scratching a sample, binding to specific chemical groups, detecting currents, or inducing reactions. In general, there are two categories of measurements: imaging and spectroscopy. Imaging involves scanning the stylus across the surface to make a topographic map and includes several modes including contact, noncontact, constant height, amplitude modulation, and frequency modulation. These modes are distinguished by the type of interaction between the stylus and the sample. Overall, the two main types of modes are AC and DC. In DC, interactions are detected by measuring the deflection of the cantilever, while in AC, the cantilever is forced to oscillate at a particular frequency and changes in the oscillation due to forces arising from the interaction between the stylus and the surface are measured (Fig. 15).

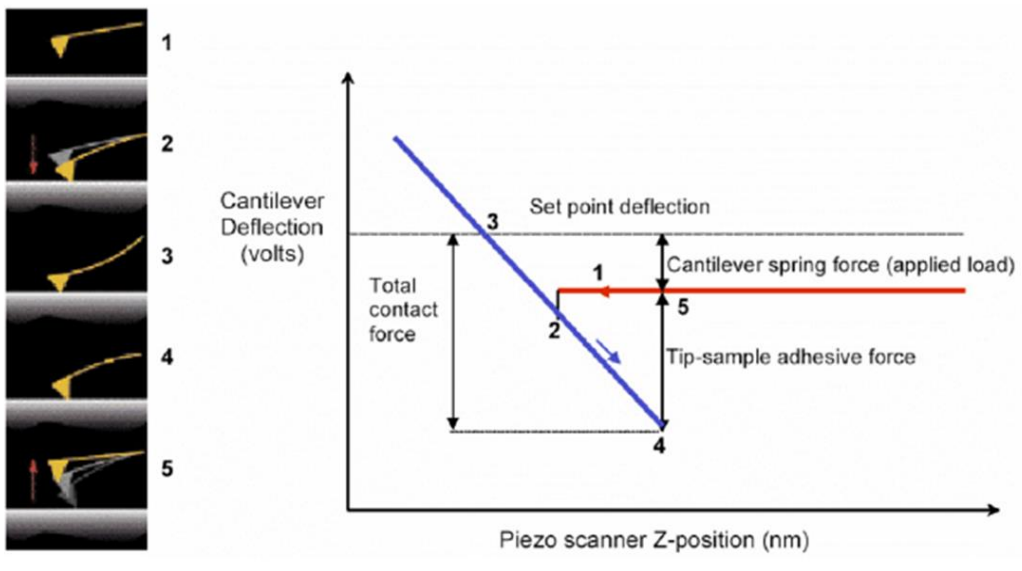

Figure 15 Force vs. Distance curve that shows how the cantilever deflects depending on the separation from the sample. The approach is in red while the withdrawal is in blue (Reprinted from Bruker Copyright 2011 Bruker Corporation).

The mode one uses in the experiment is selected based on the attractive or repulsive forces that

will occur between the sample and the tip (Fig. 16) (Braga 2011).

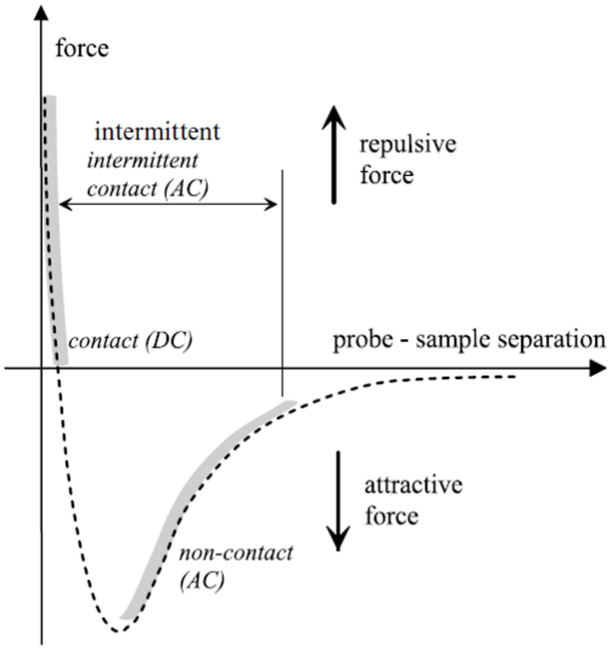

Figure 16 Plot showing which imaging modes should be used based on the tip-sample forces in the experiment (Reprinted from Braga Copyright 2011 Humana Press).

To understand the "PeakForce" operating mode used in my experiments, it is useful to review two other modes: contact and tapping. In contact mode, the tip and the sample remain in close proximity to each other throughout the raster scan. Consequently, as the cantilever deflects in response to bumps and dips in the sample, it directly registers the topography as a function of position. While overall contact mode is easy to operate, there is a fundamental flaw as a result of Newton's Third Law of motion which causes a lateral, frictional force to be present. When the lateral force becomes too high, it can then lead to sample damage or the displacement of loosely attached substances (Bruker 2011). To resolve this problem, an intermittent contact or "tapping" mode was developed. In this mode, the separation between the stylus and the surface is set to oscillate at a much higher frequency than that of the scan, to maintain only intermittent contact and release any frictional lateral forces that would otherwise accumulate. However, since the oscillations are most easily obtained by driving the cantilever near its resonance frequency, implementing a feedback loop to maintain a set oscillation amplitude is difficult to automate

because of the sensitivity of the resonance amplitude to slight frequency shifts (Bruker 2011).

To circumvent this difficulty, the "PeakForce" operating mode was used in my experiments. As for the tapping mode, the stylus intermittently contacts the sample, but at frequencies far below the resonance frequency of the cantilever (Fig. 17). PeakForce combines the calibrated force regulation of contact mode and the minimal frictional perturbation of tapping mode to allow straightforward implementation of an automated feedback loop with no damaging lateral forces.

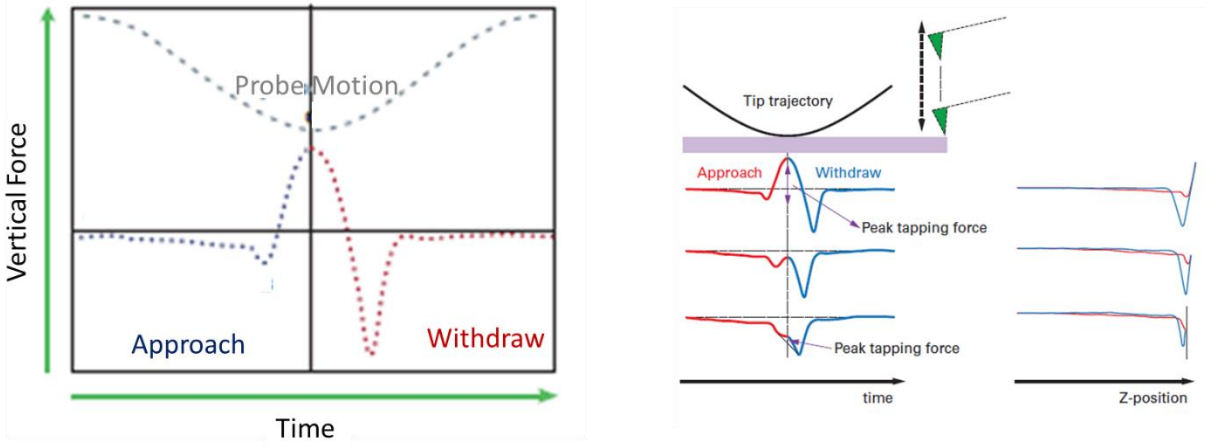

Figure 17 Graphs showing the vertical force and z-position over time for PeakForce mode. (Reprinted from Bruker Copyright 2011, 2017 Bruker Corporation).

However, since the oscillation frequencies are much lower than tapping mode, scan speeds are similar to those of tapping mode (Bruker 2011). Instead, distinct advantage of PeakForce compared to other modes is that the maximum force between the stylus and the surface can be kept relatively constant and low, which improves resolution. This makes the PeakForce mode is particularly well suited for fragile biological specimens, but it also works on a variety of other samples. In addition, the ability to limit the interaction force helps avoid damage to the stylus and the specimen. (Bruker 2017).

D. Advantages and Disadvantages

The development of AFM was in itself innovative because of the major advantages it offers over other techniques. Compared to other types of super resolution microscopy, AFM has

a relatively high signal to noise ratio while providing direct visualization of molecules. Additionally, the technique can be adapted to study a wide range of samples in a variety of different media so the integrity of bimolecular systems can be maintained as they are investigated. Furthermore, no imaging contrast agents are needed in the sample preparation which is simple and timely so there is less risk of biological activity being altered (Billingsley 2012).

However, AFM does have some several drawbacks. Slow scanning rates reduce throughput and compromise the ability to follow the progress of a reaction. In order for statistical conclusions to be meaningful, a large number of samples must also be imaged which can be lengthy because of the slow scan rates. Additionally, in the case of DNA, only simple molecules can be studied, since longer, more complicated ones become too tangled on the sample surface and confound topological analysis (Billingsley 2012).

III. Materials and Methods

A. DNA for Scanning Force Microscopy

Using PCR, 1523 base pair long DNA fragments were made with the plasmid template pUC18-LambdaLoop400, an unlabeled forward primer, and a biotin-labeled reverse primer. The amplicon was purified with a QIAQuick PCR Cleanup kit (Qiagen). Near the upstream end, the fragment had the T7A1 promoter. With respect to the promoter, the “near” operator was 261 base pairs downstream, and the “far” operator was 669 base pairs downstream. Finally, there was the lambda t1 terminator 1298 base pairs downstream.

B. Sample Preparation for Scanning Force Microscopy

Complexes with regulated elongation of RNA polymerase (REC) were prepared with DNA, CI, and RNA polymerase holoenzyme diluted in a transcription buffer (20 mM of Tris-

Glutamate, 10 mM of Mg[Glu]2, 50 mM of K[Glu], and 1 mM of DTT). DNA concentrations of 3, 2.5, 2, and 1.5 nM were tested, and the samples with 2.5 nM DNA provided the best results. Higher levels produced DNA that was too crowded to image, and for lower levels it was too sparse for efficient data collection. To drive complete occupancy of all six operators, 150 nM CI was used in the experiments . Additionally, while RNAP diluted 100 times or 150 times from the stock were used, I concluded that the 150 X dilution produced better data, since it produced a good number of RNAP bound to the DNA and facilitating transcription. Once the 2.5 nM DNA, 150 nM CI and RNA polymerase holoenzyme diluted 150 times in a transcription buffer were mixed in a test tube the sample was incubated for 25 minutes at 37°C (Fig. 18).

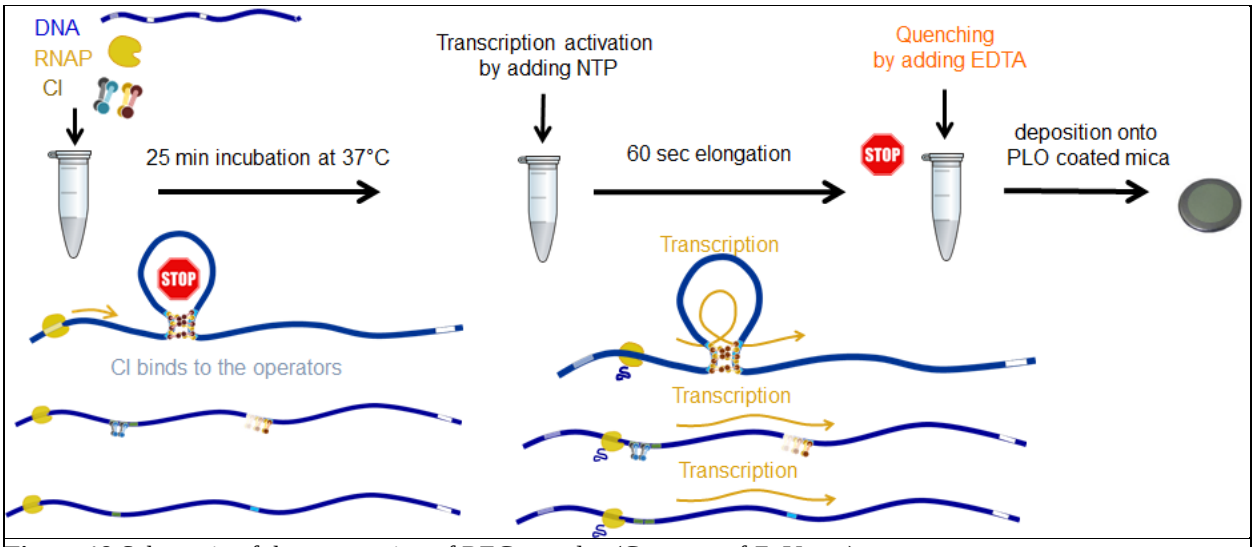

Figure 18 Schematic of the preparation of REC samples (Courtesy of Z. Voros).

Additional complexes with transcriptional elongation (TEC) were prepared in a similar manner to the REC samples without including CI (Fig. 19). Similar to the REC samples, it was determined 2.5 nM DNA, 150 nM CI and RNA polymerase holoenzyme diluted 150 times in a transcription buffer provided the best results.

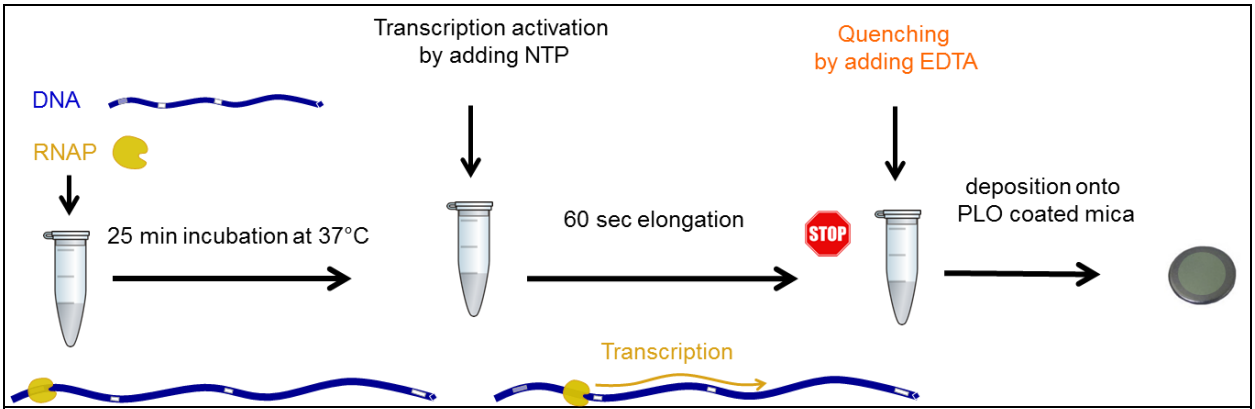

Figure 19 Schematic of the preparation of TEC samples (Courtesy of Z. Voros).

In both the REC and TEC samples, transcription was initiated by introducing NTP and letting it incubate for a set amount of time. Final concentrations of 100 µM, 10 µM, and 1 mM NTP were tested along with incubation times of 15 sec, 30 sec, 1 min, 2 min and 4 min. However, the 100 µM NTP with an incubation time of 1 min gave the best results. With other combinations, I did not see enough elongated RNAP along the DNA possibly because they either stopped at the CI position, dissociated after contacting CI, or ran off the end of the DNA. After incubation with NTP, elongation was halted by adding 250 mM EDTA to produce a final concentration of 20 mM. The EDTA-spiked sample was incubated for 15 to 30 seconds before the solution was deposited for imaging.

A freshly cleaved mica surface was first prepared for the deposition of the samples by placing 5 µl of 0.01ug/ml aqueous solution of 1000 molecular weight poly-L-ornithine (Sigma) on the surface for 2 minutes. It was then rinsed drop-wise with 700 µl of high-performance liquid chromatography grade water and dried with compressed air. Previously, 3 ug/ml aqueous solution of poly-L-ornithine 30 without EDTA was tried, but the the background was rough, and there was too much nascent RNA. Five µl of each sample were deposited on the poly-L-ornithine coated mica and incubated for 2 minutes. Subsequently, the mica was again washed with 700 µl of high-performance liquid chromatography grade water and dried with compressed air.

C. Scanning Force Microscopy and Tracing DNA Contours

Using a NanoScope MultiMode VIII AFM microscope (Bruker Nano Surfaces), images were acquired in PeakForce Tapping Mode with ScanAsyst-Air cantilevers which have a 0.4 N/m nominal spring constant (Fig. 20).

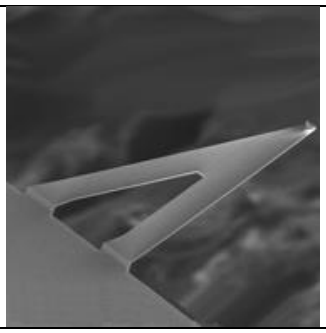

Figure 20 Image of the type of cantilever used in the experiment (Reprinted from Bruker Copyright 2017 Bruker).

Additionally, tip height was 2.5 - 8.0 μm while the front angle was 15 ± 2.5º, the back angle was 25 ± 2.5º, the side angle was 17.5 ± 2.5º, and nominal tip radius was 2 nm (Fig. 21).

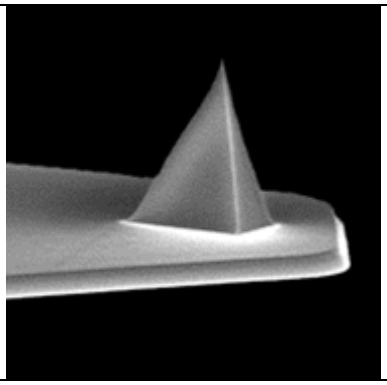

Figure 21 Image of the type of tip used in the experiment (Reprinted from Bruker Copyright 2017 Bruker).

Various areas were scanned, ranging from 3 X 3 μm^2 to 7 X 7 μm^2, with a tip speed of 2.6 μm per second (Fig. 22). Scan rate was 0.434 Hz for the 3 X 3 μm^2 image, 0.26 for the 5 X 5 μm^2, and 0.186 for the 7 X 7 μm^2 image. Additionally, resolution was 1536 X 1536 for the 3 X 3 μm^2 image, 2560 X 2560 for the 5 X 5 μm^2, and 3584 X 3584 for the 7 X 7 μm^2 image.

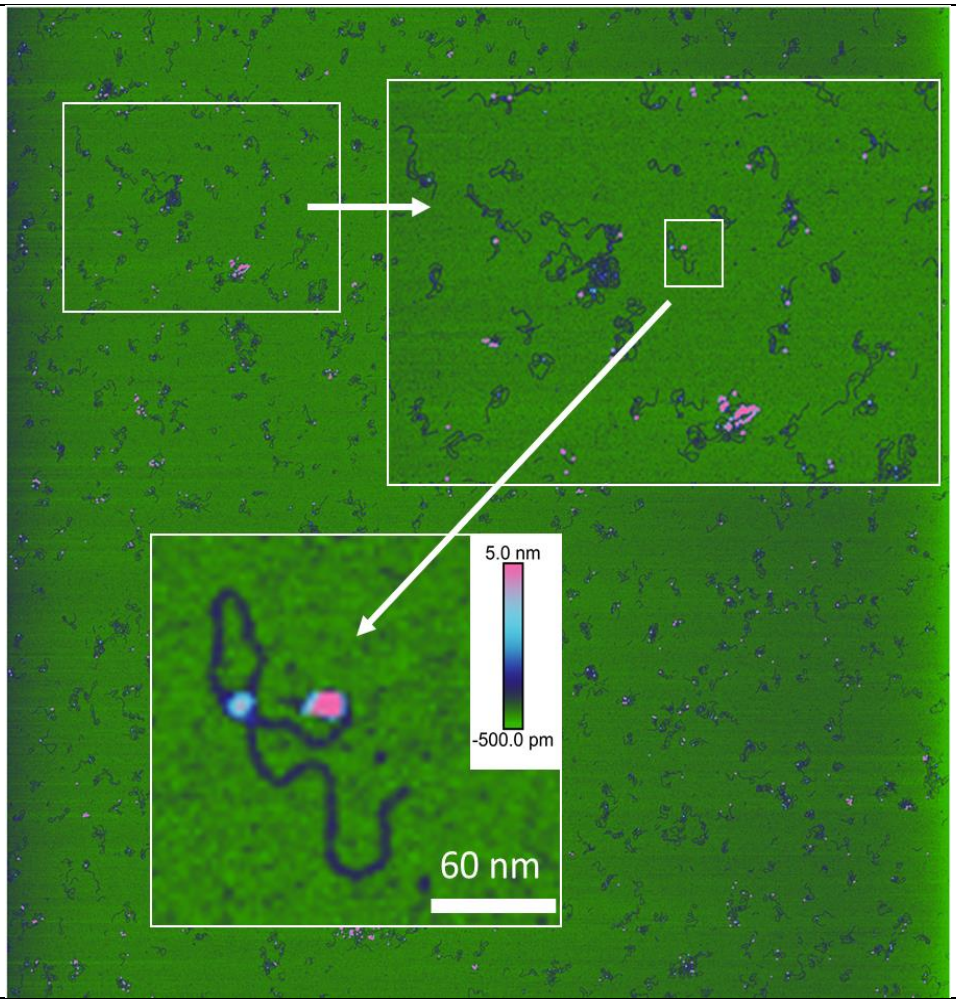

Figure 22 A high contrast image of CI mediated loops without RNAP elongation along the DNA.

Subsequently, images were filtered so the DNA molecules could then be traced using the NeuronJ plug-in of ImageJ (Fig. 23).

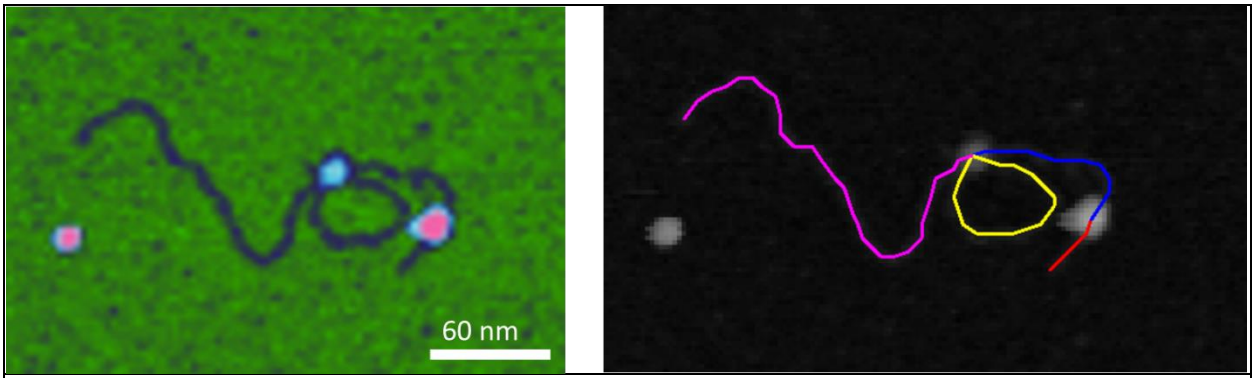

Figure 23 Tracing of a CI mediated loop without RNAP elongated along the DNA the control sample.

Measurements were taken from the endpoints to each RNAP and CI to determine their positions on the DNA. Total DNA length, loop positions and loop lengths were also measured in nanometers and used to normalize the measurement positions and converted them to bp.

IV. Results and Analysis

A. Control Imaging Shows Proper CI Binding

Using AFM, images were obtained for control, TEC and REC samples. Control samples were made with CI proteins but without NTP to verify the CI proteins were binding at the proper positions (Fig. 24).

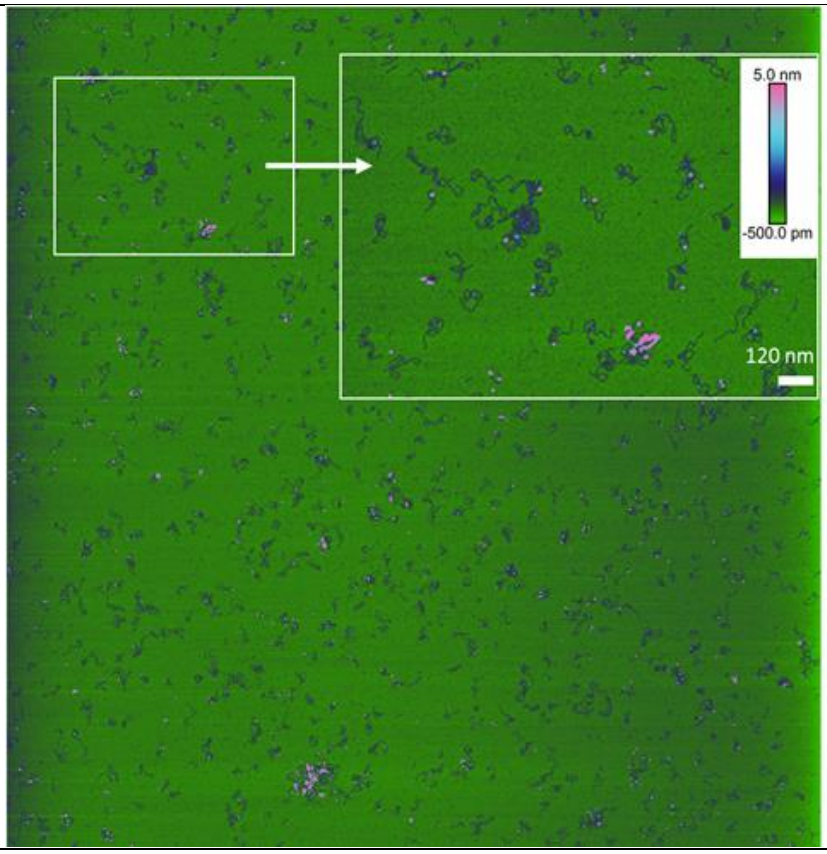

Figure 24 A high contrast image of a control sample with CI but without RNAP elongation along the DNA.

Based on the normalized data from 90 different looped and unlooped molecules in four different images, binding at the near operator, with respect to the promoter, occurred on average 389 bp away from the start of the DNA with a standard deviation of 22. Meanwhile, binding at the far operator occurred on average 879 bp away from the start of the DNA with a standard deviation of 32. Additionally, RNAP was found to be on average 93 bp away from the start of the DNA with a standard deviation of 10 (Fig. 25).

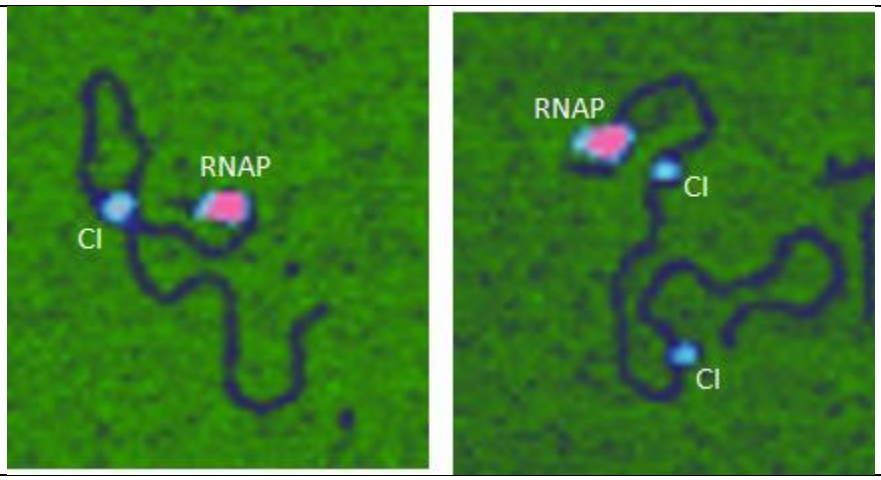

Figure 25 High contrast looped and unlooped images from control samples. RNAP is the pink circle while CI is the light blue circle. Note that on the looped molecule the CI has some pink in the middle indicating that it is bulkier on the surface than the CI on the unlooped molecules.

These positions are all in good agreement with the DNA template that was used, indicating the CI proteins were binding at the proper positions to facilitate loop formation and RNAP was correctly initiating at the promoter.

B. TEC Imaging Verifies RNAP Elongation

TEC samples were also prepared and imaged without CI to verify that in the absence of roadblocks, RNAP reaches the end of the DNA (Fig. 26).

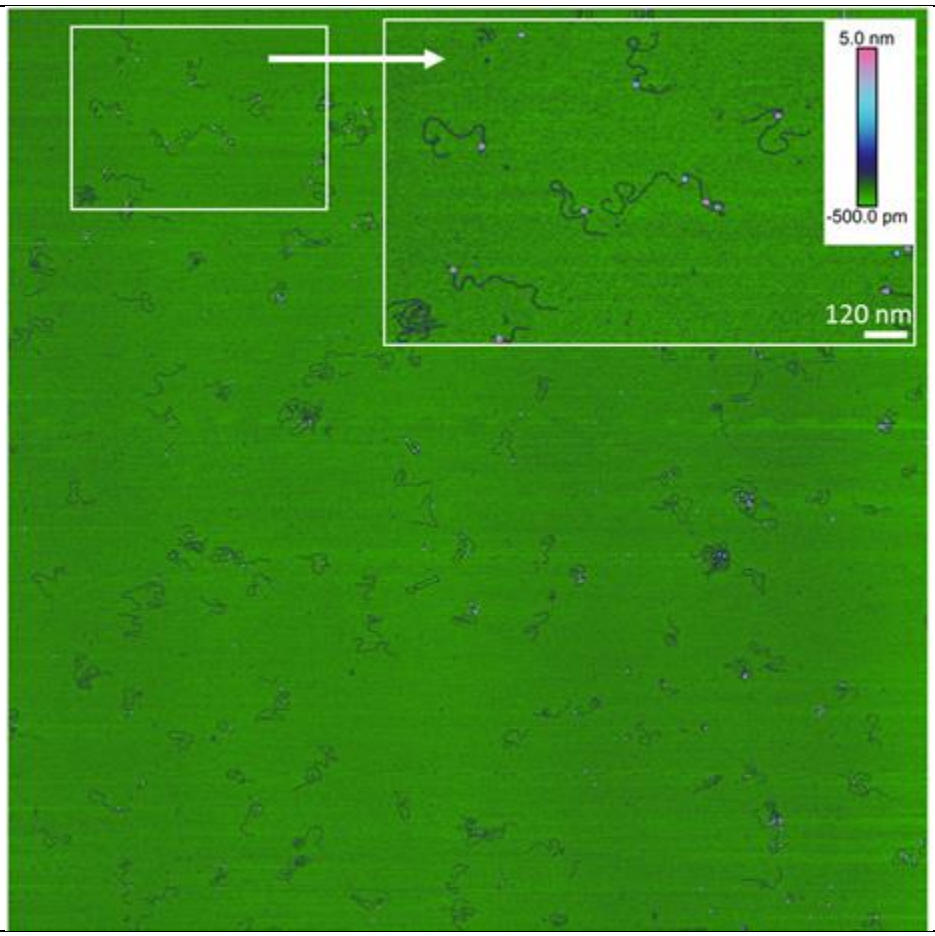

Figure 26 A high contrast image of a TEC sample without CI and with RNAP elongation along the DNA.

Based on the normalized data from 50 different molecules in three different images, RNAP was found on average to be located 508 bp away from the start of the DNA with a standard deviation of 352. Compared to the average position of 93 bp and standard deviation of 11 that occurred without transcription, the results clearly show that in the absence of roadblocks RNAP experiences elongation and can reach the end of the DNA (Fig. 27).

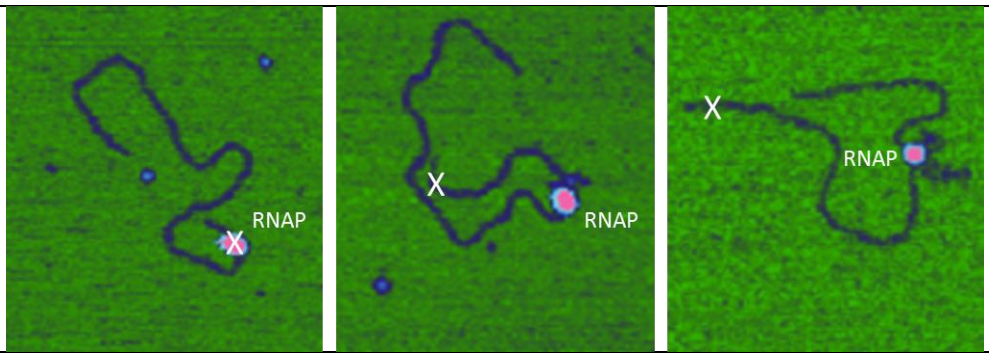

Figure 27 High contrast images from TEC samples showing RNAP elongation along the DNA. Expected promoter position is marked with a white X.

Therefore, these results demonstrate that we've set up a tractable experiment for testing if CI halts transcription.

C. REC Imaging Initially Establishes CI Looping as an Effective Roadblock

Finally, imaging of REC samples with CI proteins and NTP allowed observation of how the lambda repressor affects transcription (Fig. 28).

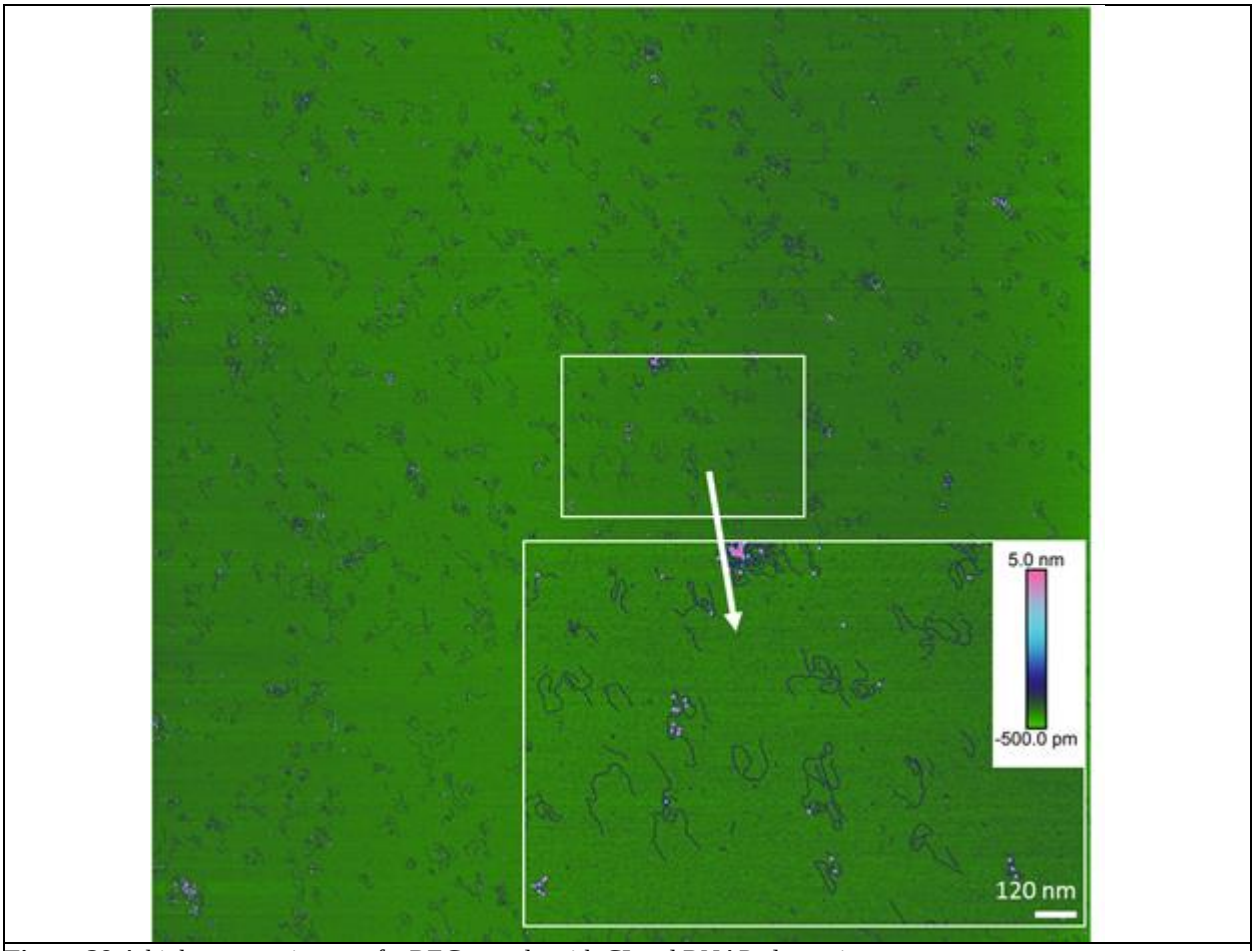

Figure 28 A high contrast image of a REC sample with CI and RNAP elongation.

Based on the normalized data from 45 different unlooped molecules in 11 different images, RNAP was found on average to be located 390 bp away from the start of the DNA with a standard deviation of 246. Therefore, the results show that unlooped molecules are not effective roadblocks as RNAP elongation occurs past the operator sites (Fig. 29).

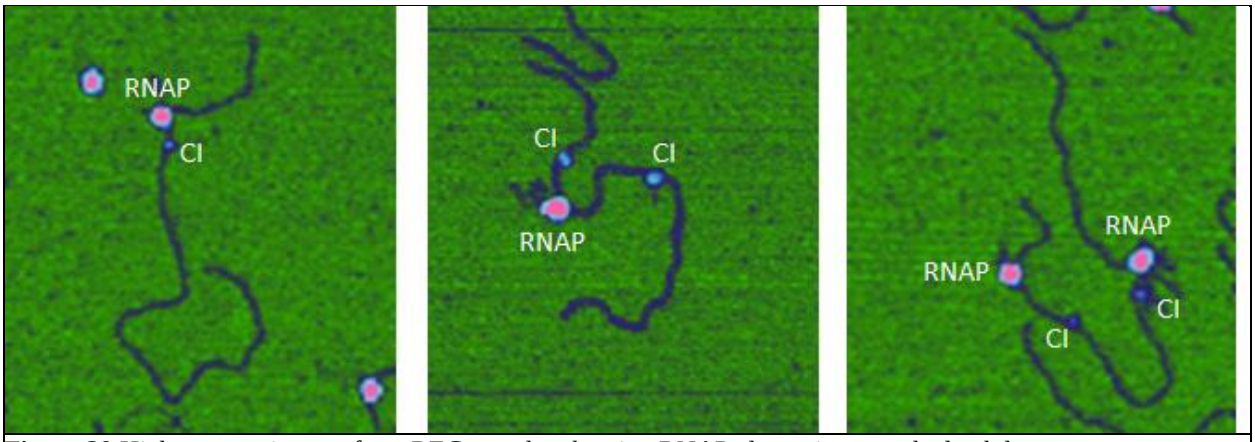

Figure 29 High contrast images from REC samples showing RNAP elongation past the lambda repressor.

Compiling these results with those of the control and TEC samples allowed a graph to be made that showed the probability of RNAP progress under different conditions (Fig. 30).

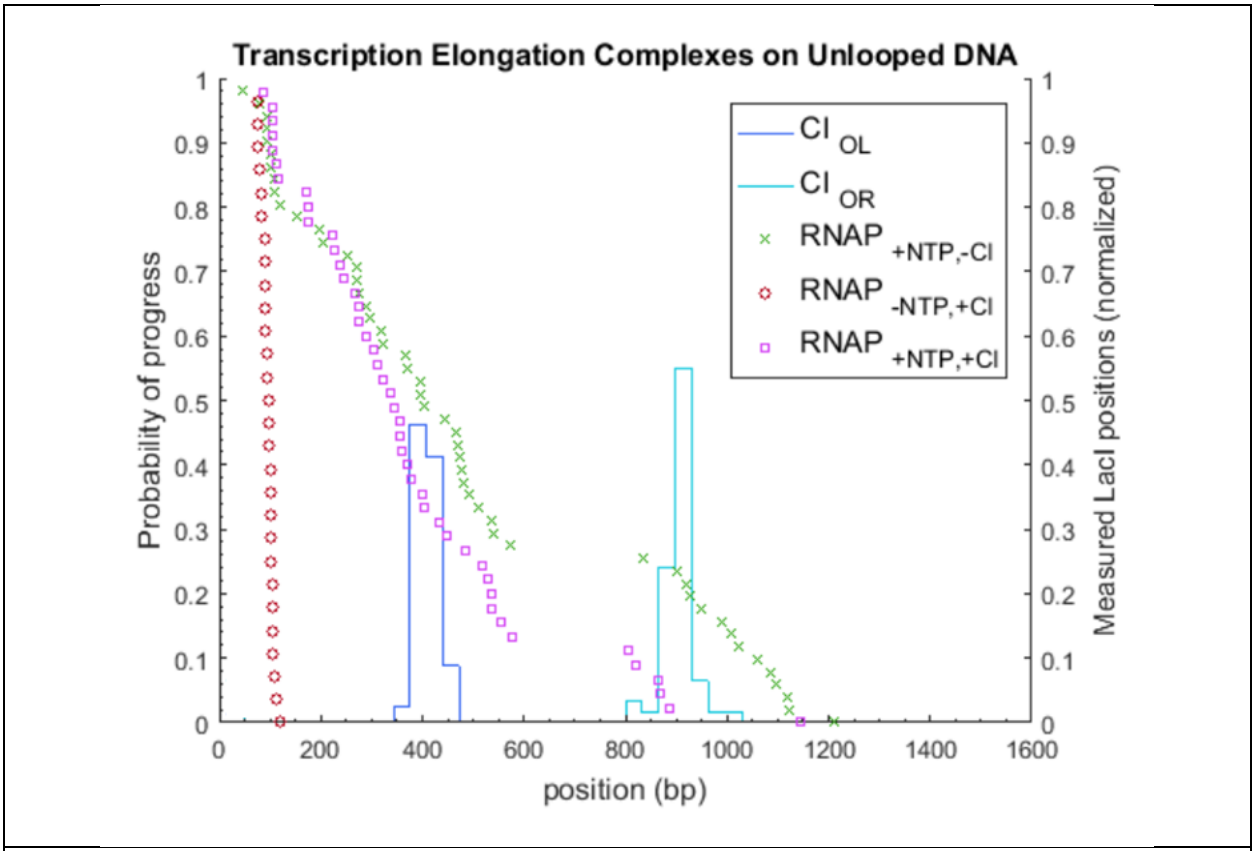

Figure 30 Graph of RNAP elongation with and without NTP and CI (Courtesy of D. Dunlap). CI binding positions for the OL and OR operators are displayed as dark blue (OL) and light blue (OL) histograms. The red circles represent the positions of RNAP without transcription initiation and show that in the absence of NTP, RNAP does not elongate. The green x's represent the positions of RNAP on molecules without CI while the purple squares represent the positions of RNAP on molecules with CI. On molecules with CI, RNAP elongates a slightly shorter distance than on molecules without CI but on both molecules RNAP can elongate past the OL and OR operator sites.

Consequently, it is shown that CI on unlooped molecules is not a significant roadblock for RNAP.

Looking at the looped molecules, normalized data from 23 different looped molecules in

10 different images showed RNAP was found on average to be located 214 bp away from the start of the DNA with a standard deviation of 118. In this case RNAP elongated a much smaller distance than the unlooped molecules, which seems to indicate that CI mediated loops are effective roadblocks (Fig. 31). This can be seen even more clearly in a distribution of these positions.

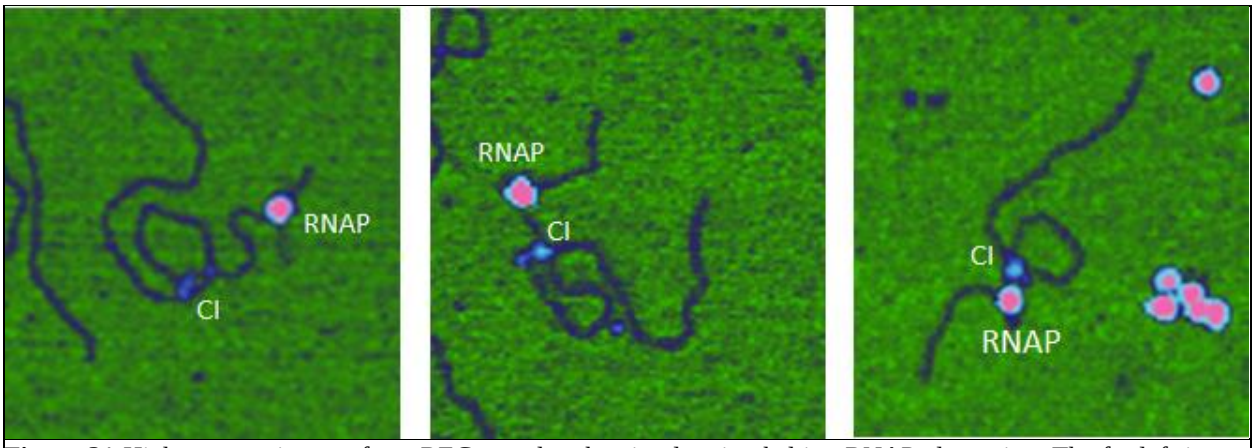

Figure 31 High contrast images from REC samples showing looping halting RNAP elongation. The far left image shows RNAP at the promoter. The middle image shows elongated RNAP at some position between the promoter and the loop. The far right image shows RNAP halted at the loop.

Compiling these results with those of the control and TEC samples also allowed a graph to be made that showed the probability of RNAP progress under different conditions (Fig. 32).

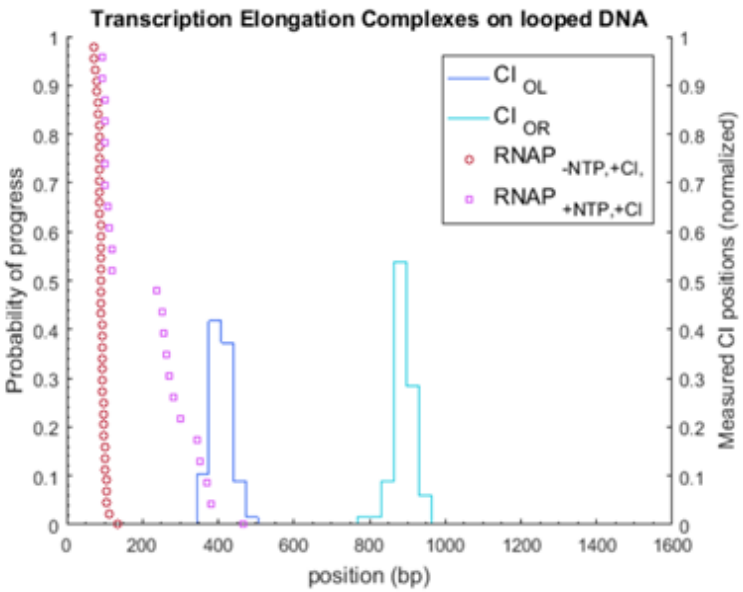

Figure 32 Graph of RNAP elongation on looped molecules with and without NTP (Courtesy of D. Dunlap). CI binding positions for the OL and OR operators are displayed as dark blue (OL) and light blue (OL) histograms. The red circles represent the positions of RNAP without transcription initiation and show that in the absence of NTP, RNAP does not elongate. The purple squares represent the positions of RNAP on molecules with CI and show that RNAP is not able to elongate past the OL operator site. However, as there wasn't a large percentage of looped molecules that were analyzed, this is not a strong conclusion.

As a result based on preliminary analysis, CI mediated loops seem to be an effective roadblock for transcriptional elongation.

V. Discussion

A. AFM Allows Direct Visualization of Roadblocks and Transcription

Because of the design of the atomic force microscope, imaging of a live system on a nanometer scale can be achieved (Braga 2011). Even though only a static snapshot of the sample could be taken, RNAP and protein position along the DNA could be measured. Depending on the location of the RNAP, transcriptional elongation could also be analyzed. Additionally, based on DNA shape, looped and unlooped molecules could be identified. Together all this information allowed conclusions to be drawn about the effect of the CI protein on transcriptional elongation.

B. CI Mediated Loops Regulate Gene Expression

Previous studies established that CI mediated looping involving the occupation of all six

operator sites represses both the lytic and lysogenic lambda bacteriophage promoters (Dodd 2001, 2004). However, while it has been known that CI operator binding directly affects gene expression, the specific effect of this roadblock on transcriptional elongation was unknown (Meyer II 1980). Results from this work suggest that the topology of the CI complex determines its effect on transcriptional elongation. Specifically, when the operator sites were occupied but the molecule remained unlooped, RNAP elongation was able to proceed past the roadblocks. However, when looping occurred under the same conditions, transcription appeared to be halted at the operator sites. This was a preliminary analysis based on the cumulative progress histogram of 23 looped molecules. In contrast, the analysis for the unlooped molecules was based on data from 46 different molecules. Further categorization of images of CI binding and topology revealed that transcription greatly reduces the number of looped molecules and the total number of molecules with a bound Lambda oligomer (Fig. 33).

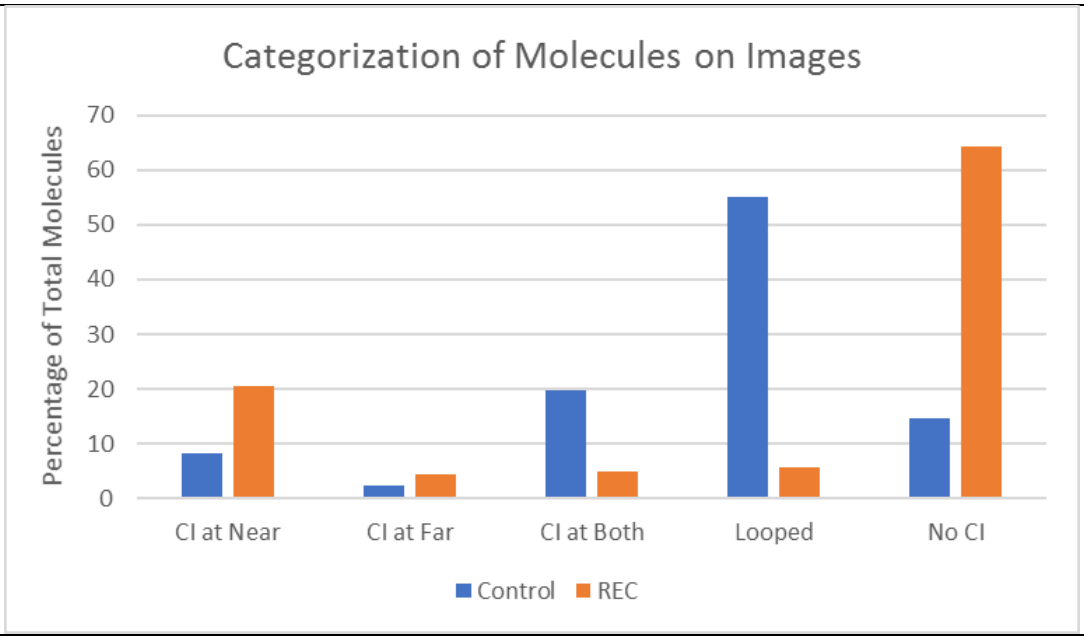

Figure 33 Categorization data for control and REC samples. The presence of transcription decreases the percentage of looped molecules and the total number of molecules with a bound CI protein. Unlike the preliminary analysis based on the cumulative progress histogram, this indicates that transcription interferes with looping and that the lambda repressor is actually not an effective roadblock for transcriptional elongation.

This additional data contradicts the first hypothesis and suggests instead that even when securing a DNA loop, lambda oligomers are not significant obstacles for transcription. To

definitively test this conclusion a more exhaustive search for molecules with RNAP beyond a looped obstacle is needed.

VI. Conclusion

The use of atomic force microscopy allowed direct visualization of the outcome of encounters between elongating RNAP complexes and obstructions constituted by CI proteins bound to DNA. Results from this study provide insight into the mechanics of a genetic switch that employs a loop mechanism in the lambda bacteriophage. Analysis of looped and unlooped molecules suggests that the CI protein is not an effective roadblock for transcriptional elongation; CI bound to unlooped molecules negligibly interferes with elongation and looping is disrupted by transcription. If lambda obstacles are of no consequence, it may be that elongating polymerases rarely converge on these sites in vivo. As a result, polymerases may not be able to disturb the regulation of the initiation of transcription from PL, PR, PRM. A consultation of the GenBank sequence data for the lambda immunogenicity region of the phage DNA, provided validation for this hypothesis as most promoters nearby were shown to diverge from the operator binding sites. As a result, OR seems to be in a relatively transcriptionally "quiet" zone. However, OL may have more elongation traffic.

VII. References

1. Aseem, Ansari. "Chemical crosshairs on the central dogma." *Nature Chemical Biology*, vol. 3, Jan. 2007, pp. 2-7. Accessed 23 Mar. 2018.
2. Billingsley, Daniel J., William A. Bonass, Neal Crampton, Jennifer Kirkham, and Neil H. Thomson. "Single-molecule studies of DNA transcription using atomic force microscopy." *Physical Biology*, vol. 9, no. 021001, 3 Apr. 2012, pp. 1-14. *IOP Science*. Accessed 22 Aug. 2017.
3. G. Binnig and C. F. Quate. “Atomic Force Microscope.” Physical Review Letters. vol. 56, no. 9, Mar 1986, pp. 930-933. Accessed 27 February 2018.
4. G. Binning and H. Rohrer. “Scanning Tunneling Microscopy.” Surface Science, vol. 126, 1983, pp. 236-244. Accessed 27 February 2018.
5. Braga, Pier C., and Davide Ricci, editors. *Atomic Force Microscopy in Biomedical Research*. Springer, Humana Press, 2011, pp. 3-29. Accessed 27 Feb. 2018.
6. Bruker Corporation. Introduction to Burker’s ScanAsyst and PeakForce Tapping AFM Technology. Bruker Corporation, 2011.

7. Bruker. PeakForceTapping, Bruker, 2017. Accessed 21 Sept. 2017.
8. Dodd, IB, AJ Perkins, D Tsemitsidis, and JB Egan. *Octamerization of lambda CI repressor is needed for effect repression of P-RM and efficient switching from lysogeny*, vol. 15, 2011, pp. 3013-22. Accessed 21 Feb. 2018.
9. Dodd, IB, KE Shearwin, AJ Perkins, T Burr, and A Hochschild. "Cooperativity in long-range gene regulation by the lambda CI repressor." *Genes Dev*, vol. 18, 2004, pp. 344-54. Accessed 21 Feb. 2018.
10. Zach Hensel, Xiaoli Weng, Arvin Cesar Lagda, and Jie Xiao. "Transcription-Factor-Mediated DNA Looping Probed by High-Resolution, Single-Molecule Imaging in Live E. coli Cells." PLoS Biol, vol. 11, no. 6, Jun 2013. Accessed 24 Feb. 2018.
11. Ann Hochschild and Mitchell Lewis. "The bacteriophage λ CI protein finds an asymmetric solution." Curr Opin Struct Biol, vol. 19, no. 1, Feb 2009, pp. 79–86. Accessed 24 Feb. 2018.
12. Kreplak, L. "Introduction to atomic force microscopy (AFM) in biology." Curr. Protoc. Protein Sci, vol. 85. 2016. Accessed 27 Feb. 2018.
13. Dale Lewis, Phuoc Le, Chiara Zurla, Laura Finzi, and Sankar Adhya. "Multilevel autoregulation of λ repressor protein CI by DNA looping in vitro." PNAS, vol. 108, no. 36, Sept 2011. Accessed 24 Feb. 2018.
14. Matthews, KS. "DNA looping." *Microbiol Rev*, vol. 56, 1992, pp. 123-26. Accessed 24 Feb. 2018.
15. Meyer, BJ, R Maurer, and M Ptashne. "Gene-regulation at the right operator (OR) of bacteriophage-lambda. 2. OR1, OR2, and OR3-their roles in mediating the effects of repressor and cro." *Mol Biol*, vol. 139, no. 15, 1980, pp. 163-94. Accessed 26 Feb. 2018.
16. Meyer, BJ and M Ptashne. "Gene-regulation at the right operator (OR) of bacteriophage-lambda. 3. Lambda-repressor directly activates Gene-regulation." *Mol Biol*, vol. 139, 1980, pp. 195-205. Accessed 26 Feb. 2018.
17. Ptashne, M. *A Genetic Switch: Phage Lambda Revisited*. 3rd ed., Cold Spring Harbor, Cold Spring Harbor Laboratory Press, 2004.
18. Revet, B, B von Wilcken-Bergmann, H Bessert, A Barker, and B Muller-Hill. "Four dimers of lambda repressor bound to two suitably spaced pairs of lambda operators form octamers and DNA loops over large distances." *Curr Biol*, vol. 9, 1999, pp. 151-54. Accessed 24 Feb. 2018.
19. AS Rose and PW Hildebrand. NGL Viewer: a web application for molecular visualization. Nucl Acids Res (1 July 2015) 43 (W1): W576-W579, 29 Apr. 2015. Accessed 26 Feb. 2018.
20. Steven Stayrook, Peera Jaru-Ampornpan, Jenny Ni, Ann Hochschild & Mitchell Lewis. "Crystal structure of the λ repressor and a model for pairwise cooperative operator binding." Nature, vol. 452, no. 24, Apr. 2008, pp. 1022-1026. Accessed 24 Feb. 2018.
21. Wilson, CJ, H Zhan, L Swint-Kruse, and KS Matthews. "The lactose repressor system: paradigms for regulation, allosteric behavior and protein folding." *Cell Mol Life Science*, vol. 64, 2007, pp. 3-16. Accessed 24 Feb. 2018.
22. Chiara Zurla, Carlo Manzo, David Dunlap, Dale E. A. Lewis, Sankar Adhya and Laura Finzi. "Direct Demonstration and Quantification of long-range DNA looping by the λ bacteriophage repressor." Nucleic Acids Research, vol. 37, no. 9, Mar. 2009, pp. 2789–2795. Accessed 24 Feb. 2018.